AGU PUBLICATIONS

Geophysical Research Letters

RESEARCH LETTER
10.1002/2016GL071546

Key Points:
- When clay is pressurized, there is a transition from plastic flow to fracture
- The rheological transitions lead to episodic gas release from a source with constant supply of gas
- The model provides an analogue to the process of intermittent mud volcano explosions

Correspondence to:
A. W. Woods,
andy@bpi.cam.ac.uk

Citation:
Rocco, S., A. W. Woods, J. Harrington, and S. Norris (2017), An experimental model of episodic gas release through fracture of fluid confined within a pressurized elastic reservoir, *Geophys. Res. Lett.*, *44*, 751–759, doi:10.1002/2016GL071546.

Received 9 JUN 2016
Accepted 23 DEC 2016
Accepted article online 29 DEC 2016
Published online 26 JAN 2017

An experimental model of episodic gas release through fracture of fluid confined within a pressurized elastic reservoir

Stefano Rocco[1], Andrew W. Woods[1], Jon Harrington[2], and Simon Norris[3]

[1]BP Institute, University of Cambridge, Cambridge, UK, [2]British Geological Survey, Nottingham, UK, [3]Radioactive Waste Management Limited, Harwell, UK

Abstract We present new experiments that identify a mechanism for episodic release of gas from a pressurized, deformable reservoir confined by a clay seal, as a result of the transition from bulk deformation to channel growth through the clay. Air is injected into the center of a thin cylindrical cell initially filled with a mixture of bentonite clay and water. For sufficiently dry mixtures, the pressure initially increases with little volume change. On reaching the yield stress of the clay-water mixture, the lid of the cell then deforms elastically and an air-filled void forms in the center of the cell as the clay is driven radially outward. With continued supply of air, the pressure continues to increase until reaching the fracture strength of the clay. A fracture-like channel then forms and migrates to the outer edge of the cell, enabling the air to escape. The pressure then falls, and the clay flows back toward the center of the cell and seals the channel so the cycle can repeat. The phenomena may be relevant at mud volcanoes.

1. Introduction

Gas migration through clay is of considerable interest for environmental engineering, marine science, petroleum geology, and soil mechanics. The accumulation and migration of gas through clay deposits can lead to mud volcano flows and release of bubbles on the seafloor [*Barry et al.*, 2012; *Boudreau*, 2012] and is relevant for the stability of methane hydrates and clathrates [*Buffett*, 2000]. One interesting application relates to the use of bentonite clay as a seal for geological disposal facilities, including radioactive waste repositories [*Pusch et al.*, 2010] where it has been proposed that bentonite seal layers could confine the waste. A considerable body of research has explored the potential behavior of such clay in geological waste repositories [e.g., *Madsen*, 1998; *Komine and Ogata*, 1994], investigating the effects of temperature changes, controls on interactions of clay and pore water including suction pressures, and the mechanical and flow properties of the clay [*Cui et al.*, 2002]. However, in some cases, as water contacts disposed material in the waste inventory, gas may be produced, primarily by corrosion of metals and degradation of organic materials, leading to pressurization and gas-clay interactions [*Sellin and Leupin*, 2013]. The dynamics and stability of such gas-clay interfaces are of considerable interest, especially if, over time, the gas pressure builds through continued production [*Harrington and Horseman*, 1999; *Shaw*, 2015].

Much of the research on the dynamics of gas migrating through clay has been carried out in high-pressure systems, in which direct visualization of the flow is difficult, and the detailed motion of the clay and gas has been inferred by measurements of stress, pore water pressure, flux, or gas breakthrough in opaque high-pressure cells [*Bennett et al.*, 2015; *Gutierrez-Rodrigo et al.*, 2014]. Such measurements have led to the generation of numerical models to describe the process of gas migration through clay [*Shao et al.*, 2015] although there are relatively few direct measurements of gas migrating through clay. As a complement to this body of work, we have developed a simplified experimental model to explore the processes that arise when gas is injected into the center of a thin cylindrical cell initially filled with a clay-water mixture. These experiments explore the response of the clay-water mixture to pressurization and displacement by the gas. Although our experiments are conducted at relatively low pressures, of order 1 atmosphere, they have exposed a potential cyclic gas release process that arises when a material with a finite yield strength is contained within an elastically deformable vessel.

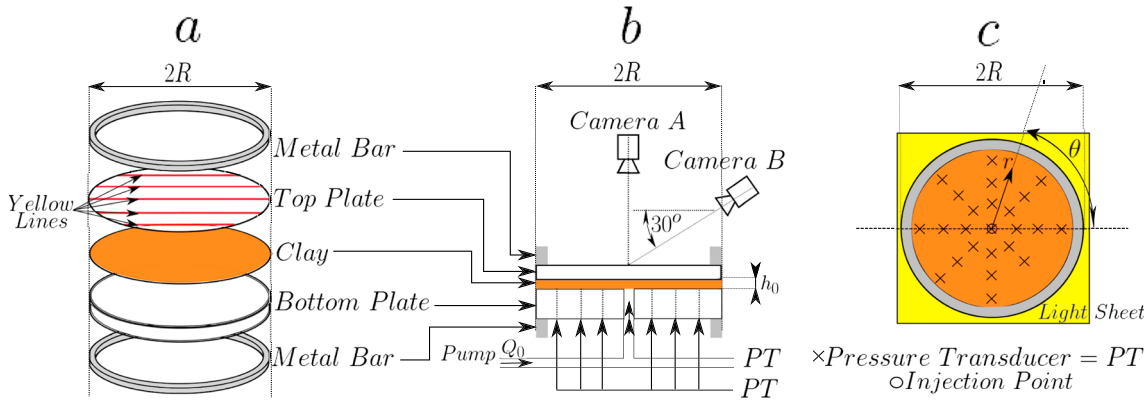

Figure 1. Schematic of the experimental apparatus.

In section 2, we describe our experimental apparatus and some details about the rheology of the bentonite-water mixtures used in our experiments. We report on a series of systematic experiments in which the clay fraction of the clay-water mixture was varied, from a dilute fluid-like mixture to a drier mixture which exhibits a yield stress [*Lagaly*, 1989] or which may fracture [*Alfaro and Wong*, 2001]. Our experiments demonstrate that there is a cyclic gas release mechanism that occurs with the clay-rich mixture and involves a series of pressurization-depressurization cycles, resulting from the balance between the slow elastic deformation of the cell and concomitant flow of clay as the system is pressurized, and the opening of a channel through the clay at a higher pressure, leading to very fast release of gas as the system decompresses. We draw some conclusions and discuss the relevance for subsurface geological waste repositories and also for observations of discrete bubble bursts at mud volcanoes.

2. Experimental Method

The experiments were carried out in a circular cylindrical cell composed of two perspex plates, each of radius of 25 cm (R_0) with a gap of 4 mm (h_0). The bottom plate is 5 cm thick while the top one is 9.1 mm thick. The bending coefficient B of the top plate has value 2.3×10^2 Pa m^3 which is much smaller than the bottom plate and so the main deformation of the cell occurs on the top plate. In setting up the experiment, the clay-water solution is spread on the bottom plate and leveled to a thickness of about 7 mm. The top plate is then placed on the mixture and the system compressed to produce a gap of approximately 4 mm. The two plates are pressed together using two metal rings of radius 24 cm and a 2×2 cm cross section to spread the stress uniformly over the perimeter of the cell. This avoids the development of a variable stress at the edge of the tank when screwing the plates together. A schematic of the apparatus is shown in Figure 1.

In order to visualize the deformation of the top plate, a grid of lines has been painted on the top boundary of the cell. During each experiment a series of photographs of the top surface was taken using a Canon D90 camera pointing at the top plate with an angle of 60° to the vertical. The setup procedure described in the previous paragraph compresses the clay, and this initial overpressure deforms the top plate. By comparing the position of the lines with respect to the initial prepressurization location, the vertical deformation ($\Delta h(r, \theta)$) can be estimated.

The experiment is backlit by an electroluminescent sheet (WȩCo LED panel 60×60 cm) and recorded from directly above the tank using a second Canon D90 camera with a 1 Hz image acquisition frequency. As air invades the cell and displaces the clay-water mixture, the light intensity increases so that the central cavity and, at later stages, fractures or channels can be visualized. In the experiments, the outer radial boundary of the cell had a coarse mesh preventing clay loss from the cell, while allowing air to leave the cell.

The clay-water solution is prepared with a food mixer which exerts a high shear stress on the clay. This breaks the bentonite platelet structures and so before running the experiment, once the clay has been placed in the cell, the system is left for 3 h so that the clay structures can become reestablished.

The clay consists of bentonite (provided by Sigma-Aldrich) mixed with water, and its physical properties are dependent on the mass fraction of clay in the mixture, $S = M_B/M_{\text{tot}}$, where M_B is the bentonite mass and M_{tot} is the total mass of the solution. In the present suite of experiments, S lies in the range $0.05 \leq S \leq 0.16$.

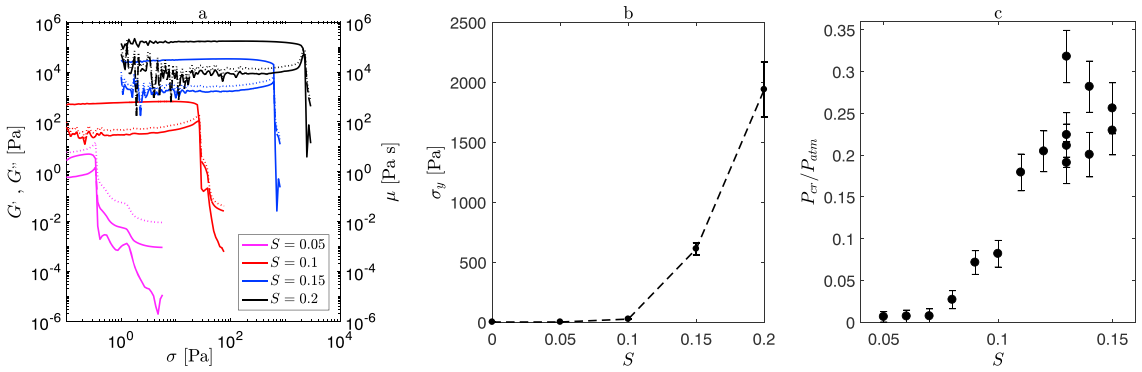

Figure 2. (a) Plot of the elastic modulus (G', solid line), the viscous modulus (G'', dashed line), and the dynamic viscosity (μ, dotted lines) measured by the rheometer at various shear stress (σ) for four different bentonite content mixtures. (b) Plot of the yield stress as a function of the clay mass fraction S. (c) Graph describing the relation between the pressure at which the fracture-like channel begins to migrate through the clay as a function of the clay mass fraction S.

We used an oscillatory rheometer (Bohlin rheometer CS-50) to measure the rheology of the clay-water mixtures (Figures 2a and 2b). At low shear stress, the bentonite behaves as an elastic material with a high and relatively constant elastic modulus (G') which increases from 1 to 10^5 Pa as S increases from 0.1 to 0.2 (solid lines in Figure 2a). Once the shear stress exceeds a critical value, the yield stress (σ_y), then the mixture deforms and the elastic modulus becomes much smaller (Figure 2a). The yield stress increases approximately exponentially with the clay content of the mixture, from about 25 Pa when $S = 0.1$ to about 2 kPa when $S = 0.2$ (Figure 2b). Beyond the yield point, the material becomes shear thinning and the effective viscosity, as measured by the rheometer, falls as the shear stress increases (dotted lines in Figure 2a).

On starting an experiment, air is pumped into a port at the center of the tank using two syringe pumps (NE-1050: World Precision Instruments) working in alternate cycles to provide an almost constant volume flow rate $Q_0 \simeq 1$ cm^3/s. The pressure (P) in the domain is measured by 24 pressure transducers with range $\pm$30 KPa and provided by Honeywell. These are connected to holes at different positions on the rigid bottom plate, one of which is located at the injection point in the center of the cell. We now describe the behavior of the system using mixtures of (section 3.1) low and (section 3.2) high clay content.

3. Experimental Results

3.1. Low Clay Content

With clay content S smaller than about 0.10, the yield stress in the clay mixture is very small, and the clay begins to flow and migrate radially outward soon after the air is injected into the centre of the cell (e.g., Figure 3a). Owing to the viscosity contrast with the air, this leads to development of a fingering instability, somewhat analogous to the Saffman-Taylor instability [*Saffman and Taylor*, 1958] as the air displaces the clay-water mixture (e.g., Figures 3b–3e). Since the clay is relatively mobile, the pressure in the cell remains relatively low and the cell deformation is small. Such fingering has been observed in earlier experiments of clay displacement in a narrow gap [cf. *Holtzman et al.*, 2012].

3.2. High Clay Content

With clay content S in excess of about 0.10, the initial viscosity of the clay mixture becomes progressively higher and the yield stress larger (Figures 2a and 2b). Figures 3f–3j illustrates the evolution of a clay-water mix ($S = 0.13$) as air is injected into the cell. After reaching the yield stress the clay spreads out in a near-radial pattern with an air void forming in the center of the cell (Figures 3f–3h). However, in Figures 3h and 3i a small fracture-like feature can also be seen to be developing in the lower left-hand side of the cell and by Figure 3j the fracture-like feature has reached the outer edge of the domain. It then releases the highly pressurized gas from the center of the cell. The clay flows back to fill the fracture-like channel and the central air void shrinks and becomes confined again. With further injection of gas the system can repressurize. Our observation of a yield stress and a fracture stress in a clay-water mixture are consistent with earlier experiments [*Marques*, 2001, *Shen and Miura*, 1999 and *Besq et al.*, 2003].

In order to analyze the evolution of these cycles in more detail, in Figures 4 and 5 we present data from another experiment using clay for which $S = 0.14$. Figure 4 (top) illustrates the evolution with time of the pressure

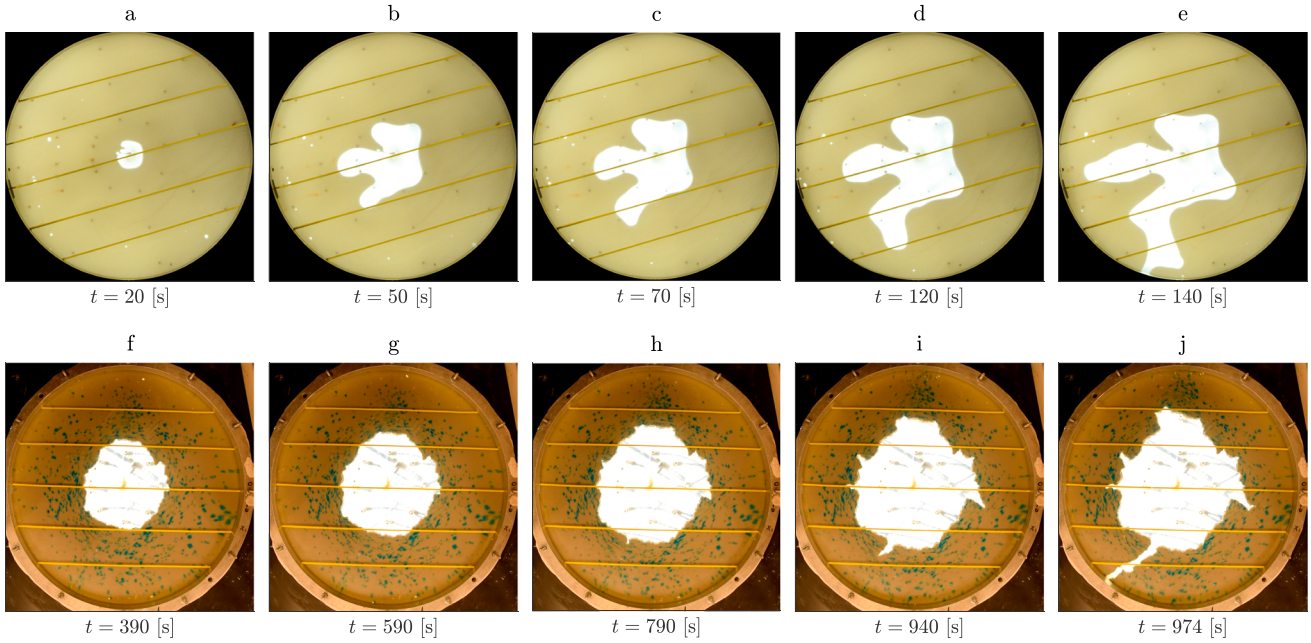

Figure 3. (a–e) Images showing the growth of the air void in an experiment for which $S = 0.07$. The clay migrates radially outward, but the interface becomes unstable and develops fingers, with a dominant finger eventually growing to the boundary of the domain allowing the gas to escape. (f–j) Series of images showing the initial nearly radial deformation of a clay-water mixture with $S = 0.13$ (Figures 3f–3h) followed by formation of a fracture-like channel (Figures 3h–3j) once the pressure surpasses a critical pressure (P_{cr}).

at the center of the cell and the average radius of the central air void, $\bar{R} = \frac{1}{2\pi}\int_0^{2\pi} R(\theta)\mathrm{d}\theta$, where $R(\theta)$ is the radius of the air void from the center of the cell at angle θ, the figure shows a series of five pressurization cycles which develop while air is supplied to the center of the cell at a near-constant rate. We also show the variation of the area of the air-filled region in the center of the cell, as measured by the average value $\bar{R^2} = (1/2\pi)\int_0^{2\pi} R^2(\theta)\mathrm{d}\theta$, as a function of the pressure in the center of the cell (Figure 4, bottom). To complement this data, in Figures 5a–5e we show a series of photographs of the deformation of the clay with time during the fifth cycle of Figure 4, and in Figures 5f and 5g we illustrate the variation of the area of the air-filled zone as a function of the pressure at the center of the cell and as a function of the height at the center of the cell to identify the conditions at which each photograph (Figures 5a–5e) was taken. At the end of each cycle, the cell has a high-pressure and large air void in the center of the cell, while a narrow channel can be seen connecting this air void to the exterior (Figure 5a). As the air escapes from the center of the cell, there is a rapid drop in pressure and in the size of the void as the deformation of the top plate decreases and clay flows back toward the center. During this phase, the channel to the exterior also becomes partially closed by the clay, isolating the remaining air void in the center of the cell (Figure 5b). Once the pressure has fallen to point B then as more air is supplied to the center of the cell, the pressure in the air-filled void builds up again. During the transition B-C, the clay is nonyielding and the air-filled void does not grow. However, on reaching point C, the pressure has become sufficient that the clay can flow and it moves outward while the upper plate of the cell deforms, as shown by points D and E. As the cell deforms the narrow channel which connected the central air void to the outer edge of the tank gradually reopens. Eventually, just beyond point E, the channel reaches the outer edge of the cell, the air escapes, and the cycle repeats.

Figure 4 (bottom) shows that there is a jump in the relation between the pressure and the size of the air void between the first pressurization cycle and the subsequent cycles. On the first cycle, the initial manually filled cell is pressurized. The clay is then redistributed and compacted within the cell during the first cycle, and toward the end of this cycle, the mesh filter at the edge of the cell fills with clay, preventing further loss of clay from the cell. As seen in Figure 4 (bottom), on subsequent cycles, the system follows a very similar deformation-pressurization path. Figure 4 (bottom) also illustrates that the pressure at which the channel to the outside edge of the clay breaks through, leading to the decompression phase, varies from cycle to cycle. It is thought that this depends on the degree of closure of the channel in the previous decompression phase. Also, the pressure at which the clay yields and the cell begins to deform varies from cycle to cycle.

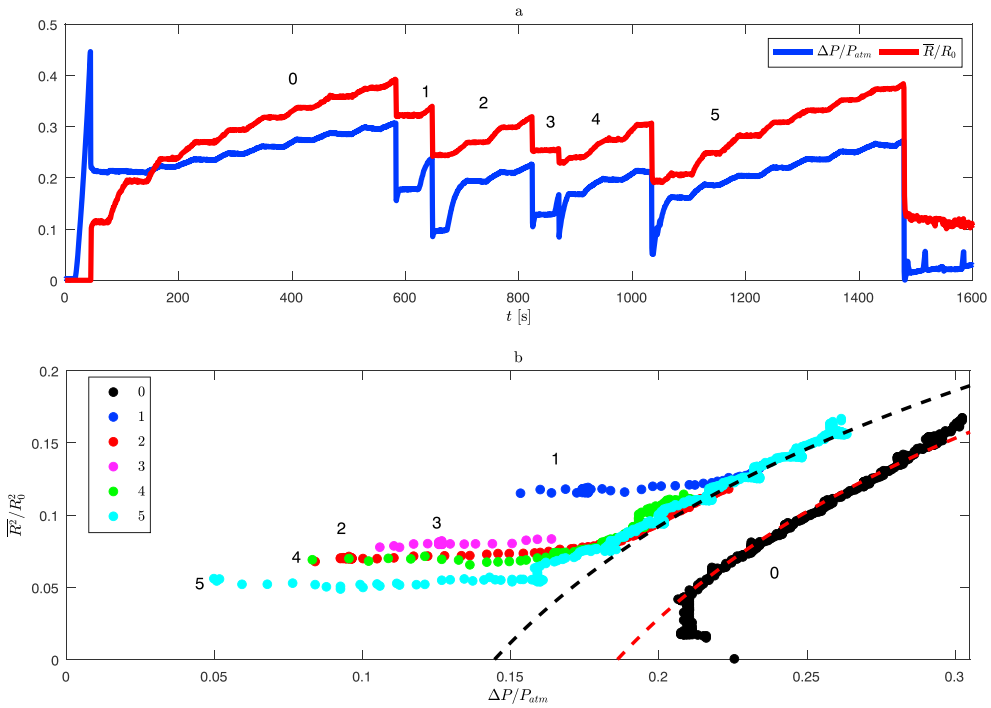

Figure 4. (top) Variation of the pressure (blue) and mean radius (red), $\bar{R}$, scaled with the radius of the cell, R_0, as a function of time during an experiment in which air is injected into a clay-water mixture with $S = 0.14$. Five pressurization-depressurization cycles may be seen. (bottom) Variation of the area of the void space in the center of the cell, $\pi\bar{R^2}$, scaled with the area of the cell, πR_0^2, as a function of the pressure at the center of the cell for the experiment shown in Figure 4 (top). After the first cycle, the system evolves along a common $\bar{R^2}$-P curve during the pressurization phase of the cycles, once the clay begins to yield and deform. The dashed lines in Figure 5 (bottom) are predicted by equations (3)–(6) using the value $B = 2.3 \times 10^2$ Pa m^3.

This is interpreted as a result of the somewhat irregular shape of the void which varies in detail from cycle to cycle. However, there is a well-defined trend relating the pressure and area of the void which we discuss later.

3.3. Variation of Breakthrough Pressure as a Function of the Clay Content

During the first cycle of each experiment it is possible to identify a transition from a nearly axisymmetric deformation where the clay is displaced radially (Figures 3f–3h) to a second phase (Figures 3h–3j) in which a narrow fracture-like channel migrates through the clay ahead of this deformation front. It is possible to identify a fracturing pressure P_{cr} (Figure 2c) as the minimum pressure at which the channel begins to form. A systematic series of experiments was carried out to determine the pressure P_{cr} as a function of the bentonite content S. Figure 2c shows that P_{cr} increases nearly exponentially with clay content, from about 8 kPa with $S = 0.1$ to about 30 kPa with $S = 0.15$.

3.4. Effect of An Outer Low Permeability Filter Ring

The origin of the cycles lies in the different time scales for injection of air, which is slow, and the release of air from the air void once the fracture-like channel reaches the outer edge of the cell, which is fast. The closure of the channel during the decompression provides a mechanism for isolating the air void during the recharge process. In order to demonstrate the dependence of the cycles on the fast release of gas along the channel, we placed a very low permeability ring around the outer edge of the cell such that the pressure jump required to drive the gas across this ring is comparable to the pressure required for the clay to yield, and we then repeated the experiments. This polyethylene ring filter (Vyon® D provided by Porvair filtration group) has a mean pore size of 16 μm and permeability estimated to be $\kappa_f \simeq 10^{-12}$ m^2. On supplying air to the cell, the pressure gradually built up within the cell and, as before, a fracture-like channel developed and grew to the outer edge of the cell. At this point, however, the flux of gas through the low permeability filter was smaller than the supply rate from the pump and so the pressure initially continued to increase until the leakage rate through the filter matched the supply rate.

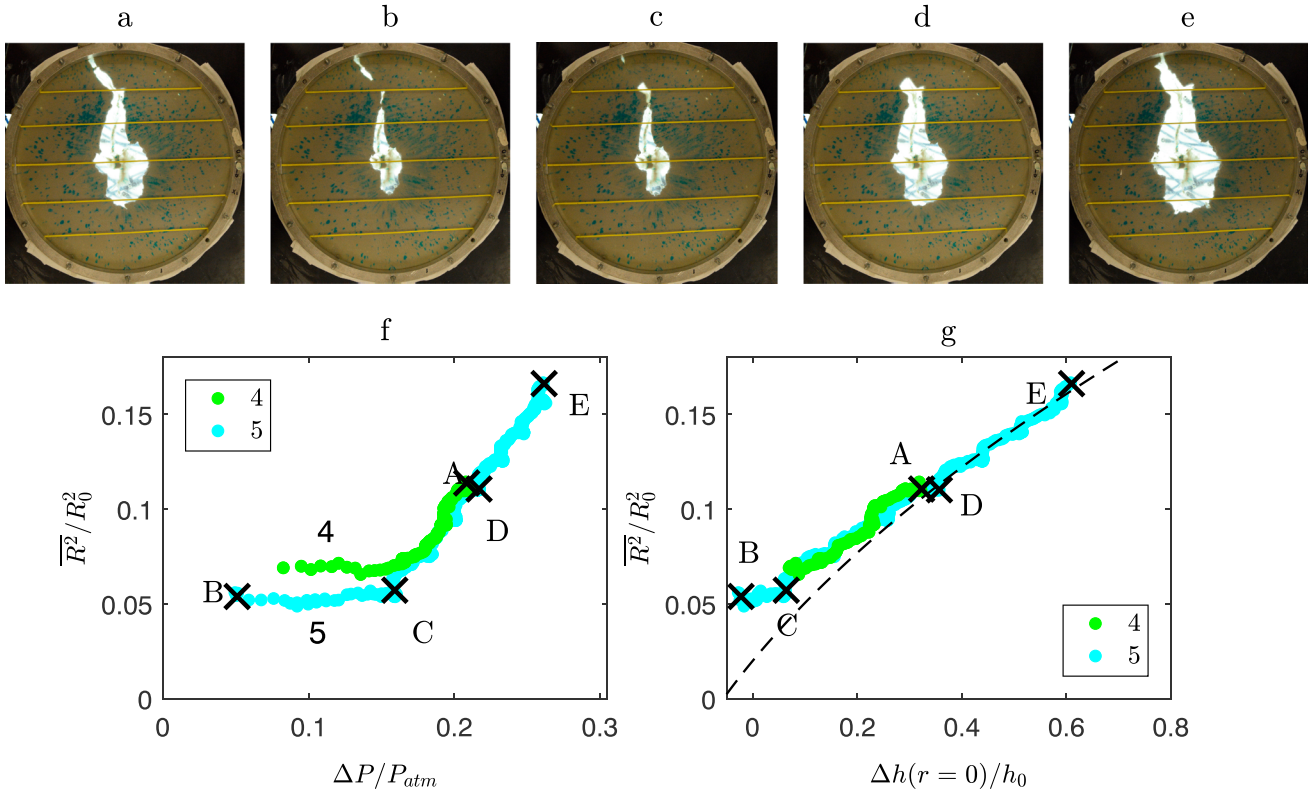

Figure 5. Series of photographs showing the evolution of the air void and clay during cycle 5 of Figure 5. The points marked A–E correspond to (a) the end of a pressurization cycle; (b) the state just after the channel reaches the outer edge of the cell and the decompression has occurred; (c) the state once the pressure has built up to the yield stress; (d) a state part way through the evolution as the clay spreads radially outward and the upper plate deforms; (e) the final pressurized state just before the fracture-like channel has reached the outer edge of the cell. Variation of the area of the air void in the center of the cell, $\pi\bar{R^2}$, scaled with the area of the cell, πR_0^2, during cycle 5, as a function of (f) the pressure at the centre of the cell and (g) the deformation at the center of the cell, showing the conditions for each of the photographs (Figures 5a–5e).

4. Discussion

The slow deformation of the cell measured in terms of the increase in the gap width, $\Delta h(r)$, relative to the uniform gap width, h_0, with zero overpressure, as a function of radius, r, may be described in terms of the overpressure within the cell, $\Delta p(r)$, and the bending moment or flexural rigidity of the upper plate of the cell, $B = 2.3 \times 10^2$ Pa m^3, according to the relation

$$\Delta p(r) = B\nabla^4(\Delta h(r)) \tag{1}$$

In equilibrium, with uniform overpressure Δp associated with the pressurization in the center of the cell, this has solution for the increase in the gap width [*Timoshenko and Woinowsky-Krieger*, 1959, equation 62]

$$\Delta h(r) = \frac{\Delta p}{64B}(R_0^2 - r^2)^2 \tag{2}$$

so that the increase in gap width at the center of the cell is related to the overpressure according to

$$\Delta p = 64B\Delta h(0)/R_o^4 \tag{3}$$

If the overpressure changes from value Δp_1 to value Δp_2, the gap between the plates changes according equation (2), leading to the expression for the change in the volume between the plates, $\Delta V = V(\Delta p_1) - V(\Delta p_2)$ given by

$$\Delta V = \frac{\pi(\Delta p_1 - \Delta p_2)}{192B}R_0^6 = \frac{\pi}{3}\left(\Delta h(0)_1 - \Delta h(0)_2\right)R_0^2 \tag{4}$$

where R_0 is the radius of the cell and $(\Delta h(0)_1 - \Delta h(0)_2)$ is the change in the gap width at the origin. If the clay is incompressible, this change in volume leads to a change in the size of the air void in the center of the cell.

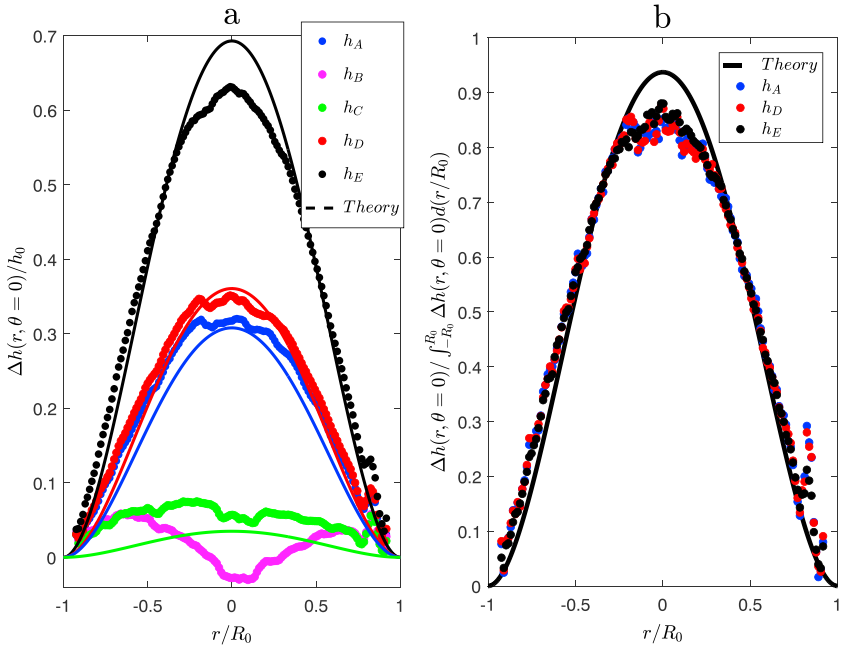

Figure 6. (a) Variation of the shape of the upper plate of the cell at points A–E of cycle 5 shown in Figure 5, illustrating the shape just prior the decompression (A), the shape following decompression (B), the onset of deformation once the clay becomes mobile (C), and followed by the growth of the void space until the clay fractures (D and E). In each case the dashed line shows the prediction of equation (2) based on the measured pressure change at the centre of the cell. (b) The rescaled shape of the deformation for each of these times is shown in comparison to the model prediction.

If the air void is modeled as being axisymmetric in the region $0 < r < R(t)$, with the clay being displaced to the outer part of the cell, $R(t) < r < R_0$, then the volume of clay in the cell V_c may be expressed as

$$V_c = \frac{\pi}{3}\Delta h(0)R_0^2\left[1-\left(\frac{R}{R_0}\right)^2\right]^3 + \pi h_0(R_0^2 - R^2) \tag{5}$$

Providing that the volume of clay in the cell remains fixed, V_c, and also that $R \ll R_0$, then it follows that as the clay is displaced outward, the gap width at the center of the cell is related to the radius of the void by the approximate relation

$$\Delta h(0) = \frac{3}{\pi R_0^2}\left\{\left[V_c - \pi h_0 R_0^2\right] + \left(3V_c - 2\pi h_0 R_0^2\right)\frac{R^2}{R_0^2}\right\} \tag{6}$$

In Figure 4 (bottom), it may be seen that after the initial deformation cycle, defined as stage 0, once the clay becomes mobile, the overpressure and hence gap width at the center of the cell (equation (3)) varies in proportion to the area of the void and on each cycle, the data follow the same curve, of the form given by equation (6). The second term on the right-hand side of equation (6), shown in square brackets, is a constant related to the fixed volume of clay in the cell and this can be estimated by fitting the curve to the data. We note that during the initial cycle of gas pressurization, defined as stage 0 in Figure 4, once the clay becomes mobile and is displaced radially outward from the center of the cell, the relation between overpressure and area of the void follows the relation given by equation (6), but with a larger constant. This is because near the end of this initial cycle, as the overpressure reaches a maximum, there is some loss of clay from the edge of the cell into the filter which then suppresses any subsequent loss of clay. As a result, during the initial cycle there is more clay in the cell and so the constant has a larger value.

The relationship between $\Delta h(0)$ and $\bar{R}^2$, the size of the cavity, is consistent with our data as shown by comparison of the dashed black line and the data in Figures 4 (bottom) and 5g. Using the value of the constant in equation (6) by matching with the data, we have compared the shape of the upper surface of the cell $\Delta h(r)$ with the model prediction (equation (2)) and this is shown in Figures 6a and 6b at points A and C–E during cycle 5 of the experiment shown in Figures 4 and 5 (A and C–E). For clarity all the data have been rescaled in

Figure 6b and compared with one dimensionless model profile. There is good agreement of the model prediction for the shape of the deformed lid with the actual data, especially given the complexity of the actual shape of the void (Figure 5).

5. Summary

In a series of experiments in which air is injected into a confined two-dimensional layer of clay, we have found that as the pressure exceeds the yield stress of the clay, the air can displace the clay-water mixture radially outward and the upper plate of the cell deforms upward elastically. This leads to a radially symmetric flow of the clay until, at a higher pressure, a fracture-like channel migrates through the clay to the outer edge of the cell. The pressurized air in the center of the cell then escapes along this channel, with an associated rapid decrease in the pressure of the cell, closure of the channel, and shrinking of the air void, as the clay spreads out. The continued injection of air into the cell then builds up the pressure of the isolated air void until the clay becomes mobile and is displaced outward again and the cycle repeats. The critical pressures at which the clay becomes mobile and at which the fracture-like channel opens up do vary from cycle to cycle, owing to the irregular shape of the air void and to the nonuniqueness of the fracture healing process during decompression.

The experiments have implications for a number of geophysical processes involving the pressurization of non-Newtonian materials by injection or production of gas, and the ensuing episodic release of the gas. The process may be responsible for the periodic release of biogenic gas which accumulates in mud deposits on the seafloor or for the episodic release of gas in mud volcano systems, as methane builds up in a subsurface reservoir until reaching a critical pressure to fracture the mud. For example, *Feseker et al.* [2014] report on four eruption events emitting about 10^4 m^3 methane over a 430 day survey of the Hakon Mosby Sea Volcano. The fractional change in volume, ΔV, required to pressurize the clay up to the fracturing pressure ΔP is given by $\Delta V/V = \Delta P/\beta$. If we assume the mud has a fracture stress with values of 10^5 Pa [*Marques*, 2001] to 10^7 Pa [*Donohew et al.*, 2000], then if the gas accumulates at depths of a several hundred meters over a volume of $V \sim 10^8$ m^3, for example, perhaps extending of order $1-5 \times 10^3$ m in lateral scale [*Shirzaei et al.*, 2015], then with a bulk modulus of order $\beta = 3.6 \times 10^{10}$ Pa [*Poletto and Miranda*, 2004, Table 4.2], we predict that the volume which can erupt, ΔV will be in the range $10^3 - 10^5$ m^3, analogous to observations. Following fracture of the confining clay, this excess gas may migrate and erupt at the surface. In the case of a geological waste repository in which the waste material is sealed within a clay layer or clay-based engineered barrier, the accumulation of gas following generation within the repository may lead to an increase in pressure until eventually fracturing of the confining clay occurs. This could generate transient high permeability pathways which enable relatively long-range gas transport even though the clay is an inherently low permeability medium.

Acknowledgments
All the experiment results and data about the experiments presented or described in the graphs or in the text in this paper are available by request from A.W. Woods (andy@bpi.cam.ac.uk; BP Institute, Madingley Rise, Madingley Road, Cambridge, England, CB3 OEZ).

References

Alfaro, M. C., and R. C. Wong (2001), Laboratory studies on fracturing of low-permeability soils, *Can. Geotech. J.*, *38*(2), 303–315.
Boudreau, B. (2012), The physics of bubbles in surficial, soft, cohesive sediments, *Mar. Petrol. Geol.*, *38*(1), 1–18.
Barry, M. A., B. P. Boudreau, and B. D. Johnson (2012), Gas domes in soft cohesive sediment, *Geology*, *40*(4), 379–382.
Bennett, D. P., R. J. Cuss, P. J. Vardon, J. F. Harrington, M. Sedighi, and H. R. Thomas (2015), Exploratory data analysis of the Large Scale Gas Injection Test (Lasgit) dataset, focusing on second-order events around macro-scale gas flows, *Geol. Soc. London Spec. Publ.*, *415*(1), 225–239.
Besq, A., C. Malfoy, A. Pantet, P. Monnet, and D. Righi (2003), Physicochemical characterisation and flow properties of some bentonite muds, *Appl. Clay Sci.*, *23*(5), 275–286.
Buffett, B. A. (2000), Clathrate hydrates, *Annu. Rev. Earth Planet. Sci.*, *28*(1), 477–507.
Cui, Y. J., M. Yahia-Aissa, and P. Delage (2002), A model for the volume change behavior of heavily compacted swelling clays, *Eng. Geol.*, *64*(2), 233–250.
Donohew, A. T., S. T. Horseman, J. F. Harrington, J. D. Cotter-Howells, L. S. Campbell, E. Valsami-Jones, M. Batchelder (2000), Gas entry into unconfined clay pastes at water contents between the liquid and plastic limits, in *Environmental Mineralogy: Microbial Interactions, Anthropogenic Influences, Contaminated Land and Waste Management*, pp. 369–394, Mineralogical Society of Great Britain & Ireland, London.
Feseker, T., A. Boetius, F. Wenzhofer, J. Blandin, K. Olu, D. Yoerger, R. Camilli, C. German, and D. de Beer (2014), Eruption of a deep-sea mud volcano triggers rapid sediment movement, *Nat. Commun.*, *5*, 5385, doi:10.1038/ncomms6385.
Gutierrez-Rodrigo, V., M. V. Villar, P. L. Martin, F. J. Romero, and J. M. Barcala (2014), Gas-breakthrough pressure of FEBEX bentonite, *Geol. Soc. London, Spec. Publ.*, *415.1*, 47–57.
Harrington, J. F., and S. T. Horseman (1999), Gas transport properties of clays and mudrocks, *Geol. Soc. London, Spec. Publ.*, *158.1*, 107–124.
Holtzman, R., M. L. Szulczewski, and R. Juanes (2012), Capillary fracturing in granular media, *Phys. Rev. Lett.*, *108.26*, 264504.
Komine, H., and N. Ogata (1994), Prediction for swelling characteristics of compacted bentonite, *Can. Geotech. J.*, *33*(1), 11–22.
Lagaly, G. (1989), Principles of flow of kaolin and bentonite dispersions, *Appl. Clay Sci.*, *4*(2), 105–123.
Madsen, F. T. (1998), Clay mineralogical investigations related to nuclear waste disposal, *Clay Miner.*, *33*(1), 109–129.
Marques, F. O. (2001), Flow and fracturing of clay: Analogue experiments in bulk pure shear, *Mem. Geol. Soc. Am.*, *193*, 261–270.

Poletto, F., and F. Miranda (2004), *Seismic While Drilling, Fundamentals of Drill-bit Seismic for Exploration, Handbook of Geophys. Explor.*, vol. 35, Elsevier, Amsterdam.

Pusch, R., J. Kasbohm, and H. T. M. Thao (2010), Chemical stability of montmorillonite buffer clay under repository-like conditions—A synthesis of relevant experimental data, *Appl. Clay Sci.*, *47*(1), 113–119.

Saffman, P. G., and G. Taylor (1958), The penetration of a fluid into a porous medium or Hele-Shaw cell containing a more viscous liquid, *Proc. R. Soc. London, Ser. A*, *245*(1242), 312–329.

Sellin, P., and O. X. Leupin (2013), The use of clay as an engineered barrier in radioactive-waste management—A review, *Clays Clay Miner.*, *61*(6), 477–498.

Shaw, R. P. (Ed.) (2015), *Gas Generation and Migration in Deep Geological Radioactive Waste Repositories*, vol. 415, Geol. Soc. of London, London, U. K.

Shao, H., W. Xu, P. Marschall, O. Kolditz, and J. Hesser (2015), Numerical interpretation of gas-injection tests at different scales, *Geol. Soc. London Spec. Publ.*, *415*(1), 203–212.

Shen, S. L., and N. Miura (1999), Soil fracturing of the surrounding clay during deep mixing column installation, *Soils Found. Jpn. Geotech. Soc.*, *39*(5), 13–22.

Shirzaei, M., M. L. Rudolph, and M. Manga (2015), Deep and shallow sources for the Lusi mud eruption revealed by surface deformation, *Geophys. Res. Lett.*, *42*, 5274–5281, doi:10.1002/2015gl064576.

Timoshenko, S. P., and S. Woinowsky-Krieger (1959), *Theory of Plates and Shells*, McGraw-Hill, New York.